The Astrophysical Journal Letters, 715:L1–L5, 2010 ??? doi:10.1088/2041-8205/715/1/L1

MAGNETIC CYCLES IN GLOBAL LARGE-EDDY SIMULATIONS OF SOLAR CONVECTION

Mihai Ghizaru[1], Paul Charbonneau[1], and Piotr K. Smolarkiewicz[2]
[1] Département de Physique, Université de Montréal, C.P. 6128 Succ. Centre-ville, Montréal, Qc, H3C-3J7, Canada
[2] National Center for Atmospheric Research, Boulder, CO 80307, USA
Received 2010 February 21; accepted 2010 April 28; published 2010 ???

ABSTRACT

We report on a global magnetohydrodynamical simulation of the solar convection zone, which succeeds in generating a large-scale axisymmetric magnetic component, antisymmetric about the equatorial plane and undergoing regular polarity reversals on decadal timescales. We focus on a specific simulation run covering 255 years, during which 8 polarity reversals are observed, with a mean period of 30 years. Time–latitude slices of the zonally averaged toroidal magnetic component at the base of the convecting envelope show a well-organized toroidal flux system building up in each solar hemisphere, peaking at mid-latitudes and migrating toward the equator in the course of each cycle, in remarkable agreement with inferences based on the sunspot butterfly diagram. The simulation also produces a large-scale dipole moment, varying in phase with the internal toroidal component, suggesting that the simulation may be operating as what is known in mean-field theory as an $\alpha\Omega$ dynamo.

Key words: convection – magnetohydrodynamics (MHD) – Sun: activity – Sun: dynamo

1. NUMERICAL SIMULATIONS OF CONVECTION AND THE SOLAR DYNAMO

It is now generally agreed upon that the solar activity cycle ultimately owes its existence to the inductive action of fluid flows pervading the solar interior. However, the turbulent nature of these internal flows yields a computationally challenging problem. Following the advent of high-performance computing, parallelized versions of the Glatzmaier (1984) simulation model made high-resolution calculations possible attaining a strongly turbulent regime (see Miesch & Toomre 2009, and references therein). Dynamo action in these simulations proved very efficient at producing small-scale magnetic fields, but failed to generate a spatially well-organized large-scale component (Brun et al. 2004). Toward this end, the presence of a stably stratified tachocline-like layer, where significant rotational shear could persist, was shown by Browning et al. (2006) to be an important, possibly essential ingredient. These authors succeeded in producing a large-scale magnetic component, antisymmetric about the equator and persistent on yearly timescales. However, no polarity reversals were observed over the 8 year time span of these simulations.

Herein, we report on a series of global magnetohydrodynamical (MHD) simulations of the solar convection zone (SCZ), conceptually similar to those referenced above, that do produce well-organized large-scale magnetic fields undergoing regular cyclic polarity reversals on decadal timescales. Our model integrates the anelastic form of the MHD equations (Glatzmaier 1984) in a thick, rotating spherical shell of electrically conducting fluid. We use a modified version of the general-purpose hydrodynamical simulation code EULAG (see Prusa et al. 2008 for a review) in which we have introduced magnetic fields and a solar-like, spherically symmetric stratification of the static ambient state. Our overall simulation setup is similar to that in Browning et al. (2006). The solution domain spans the range $0.61 \leqslant r/R_\odot \leqslant 0.96$, covering 3.4 density scale heights and across which we force the solar heat flux. The ambient stratification is convectively stable in the bottom portion of the domain ($0.61 \leqslant r/R_\odot \leqslant 0.71$) and unstable above. Stress-free boundary conditions are imposed at the top and bottom boundaries, with the magnetic field constrained to remain radial (magnetically open). We defer an exposition of the model formulation to a forthcoming publication, with only a few highlights provided below.

The anelastic hydrodynamic SCZ model of Elliot & Smolarkiewicz (2002) is cast in an anholonomic time-dependent curvilinear framework of Prusa & Smolarkiewicz (2003) and extended to MHD. The governing equations take the form

$$\begin{aligned}
\frac{D\mathbf{v}}{Dt} &= -\nabla\pi - \mathbf{g}\frac{\theta'}{\theta_o} + 2\mathbf{v}' \times + \frac{1}{\mu\rho_o}(\mathbf{B}\cdot\nabla)\,\mathbf{B} + \mathcal{D}_\mathbf{v}, \\
\frac{D\theta'}{Dt} &= -\mathbf{v}\cdot\nabla\theta_e + \mathcal{H} - \alpha\theta', \\
\frac{D\mathbf{B}}{Dt} &= -\nabla\pi^* + (\mathbf{B}\cdot\nabla)\,\mathbf{v} - \mathbf{B}(\nabla\cdot\mathbf{v}) + \mathcal{D}_\mathbf{B}, \\
\nabla\cdot(\rho_o\mathbf{v}) &= 0,\ \nabla\cdot\mathbf{B} = 0,
\end{aligned} \tag{1}$$

where $\mathbf{v}$ and $\mathbf{B}$ denote vectors of the physical velocity and of the magnetic field, measurable at every point of the spherical shell in a local Cartesian frame tangent to the lower surface of the shell, and θ is the potential temperature (tantamount to the specific entropy, $s = c_p \ln\theta$). Subscripts "o" refer to the basic isentropic state with density satisfying hydrostatic balance with $\mathbf{g} \propto r^{-2}$. Primes denote deviations from a prescribed ambient state different, in general, than the basic state (Prusa et al. 2008). In the momentum equation, π is a density-normalized pressure perturbation inclusive of the magnetic pressure and centrifugal force, and $\mathcal{D}_\mathbf{v}$ symbolizes viscous dissipation. In the entropy equation, $\mathcal{H}$ combines heat sink/sources due to radiation, diffusion, and viscous heating. A weak Newtonian cooling (here $\alpha = 2 \times 10^{-8}\ \mathrm{s}^{-1}$) damps entropy departures from the ambient stable/unstable thermodynamic profile in the tachocline/SCZ. In the induction equation, the gradient of potential π^* denotes an auxiliary term introduced to assure $\nabla\cdot\mathbf{B} = 0$ in numerical integrations, and $\mathcal{D}_\mathbf{B}$ is a shorthand for magnetic diffusion. All other symbols have their usual meaning.

Using the mass continuity equation and the solenoidality constrain on $\mathbf{B}$, the system (1) is rewritten as a set of Eulerian conservation laws and solved using the non-oscillatory forward-in-time (NFT) approach, widely documented in the literature; see Prusa et al. (2008) and Smolarkiewicz & Szmelter (2009) for

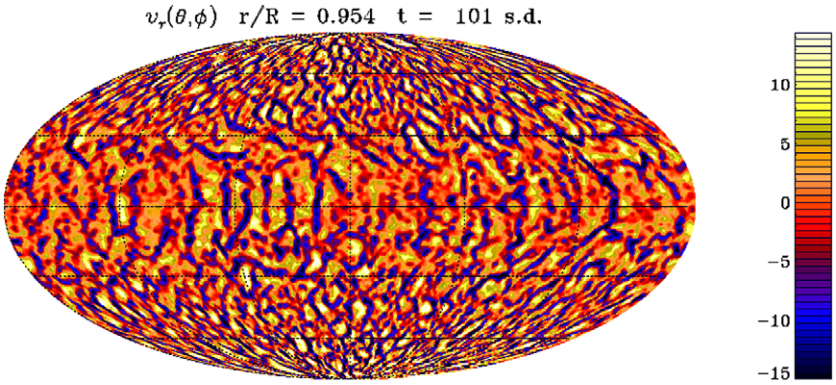

Figure 1. Radial component of the flow velocity at $r/R_\odot = 0.954$, near the domain top, in an $N_\phi \times N_\theta \times N_r = 256 \times 128 \times 93$ simulation. The results are plotted in Mollweide projection, with the color scale coding the flow speed in m s^{-1}. Peak radial flow speed occurs in downflow lanes, and here can reach ∼25 m s^{-1}.

recent reviews and discussions. In essence, the resulting system of the partial differential equation is viewed as

$$\frac{\partial \rho^* \Psi}{\partial t} + \nabla \cdot (\mathbf{V}^* \Psi) = \mathbf{R}, \tag{2}$$

where Ψ denotes the vector of prognosed-dependent variables (components of $\mathbf{v}$, $\mathbf{B}$, and θ'), $\rho^* = G\rho_o$ combines the anelastic density and the Jacobian of coordinate transformation, $\mathbf{V}^* = \rho^* \mathbf{x}$ is an effective advective velocity, with $\mathbf{x}$ symbolizing the contravariant velocity of the actual curvilinear coordinates, and $\mathbf{R}$ is a shorthand for the associated right-hand side inclusive of the metric forces (viz., Christophel's terms). The model algorithm for a discrete integration of Equation (2) in the time–space continuum relies on the implicit trapezoidal rule approximation. It is formulated in the spirit of

$$\Psi_{\mathbf{i}}^{n,\nu} = \widehat{\Psi}_{\mathbf{i}} + \frac{\delta t}{2} \mathbf{L}\Psi \Big|_{\mathbf{i}}^{n,\nu} + \frac{\delta t}{2} \mathbf{N}\Psi \Big|_{\mathbf{i}}^{n,\nu-1} - \nabla \Phi \Big|_{\mathbf{i}}^{n,\nu}, \tag{3}$$

with n, $\mathbf{i}$, and δt marking discrete locations in the model $(t, \mathbf{x})$ domain and a temporal increment, $\mathbf{L}$ and $\mathbf{N}$ denoting linear and nonlinear parts of the right-hand side operators, $\Psi \equiv (\mathbf{v}, \theta', \mathbf{B})$, $\Phi \equiv 0.5\delta t(\phi, \phi, \phi, 0, \phi^*, \phi^*, \phi^*)$, and $\nu = 1, \ldots, m$ numbering the fixed point iterations. With all prognostic-dependent variables co-located, the execution of Equation (3) invokes its local algebraic inversion with respect to $\Psi_{\mathbf{i}}^{n,\nu}$; after which, enforcing discretized mass continuity and magnetic field solenoidality on the components $\mathbf{v}$ and $\mathbf{B}$ leads to the associated discrete elliptic problems for ϕ and ϕ^*. These are solved with a robust, preconditioned non-symmetric Krylov-subspace solver (Smolarkiewicz et al. 1997, 2004), essentially completing the model algorithm.

A key element of the NFT approach implemented in EULAG is a universally second-order-accurate (in time and space) NFT advection operator MPDATA that forms the explicit element $\widehat{\Psi}_{\mathbf{i}} \equiv \mathcal{A}_{\mathbf{i}}(\Psi^{n-1} + 0.5\delta t \mathbf{R}^{n-1}, \widetilde{\mathbf{V}}^*)$ of Equation (3), with $\mathcal{A}$ and $\widetilde{\mathbf{V}}^*$ denoting, respectively, the advection operator and a solenoidal $\mathcal{O}(\delta t^2)$ estimate of $\mathbf{V}^*$ at $t^{n-1/2}$. MPDATA is a finite-volume, high-resolution multi-pass (iterative) upwind scheme, already well reviewed in the literature; see Smolarkiewicz & Szmelter (2009), and references therein. A particular feature of MPDATA important for the present study is its proven dissipative property mimicking the action of explicit subgrid-scale turbulence models where the flow is under-resolved (Domaradzki et al. 2003). Such calculations relying on the properties of non-oscillatory differencing are referred to in the literature as implicit large-eddy simulations, or ILES. While minimizing the computational effort, they tend to maximize the effective Reynolds number of simulations (Waite & Smolarkiewicz 2008; Piotrowski et al. 2009). In the experiments reported here, we retained only the radiative diffusion in the $\mathcal{H}$ forcing term on the right-hand side of the entropy equation in (1), while delegating the entire system dissipativity to ILES. This effects in magnetic Prandtl number ≈1 and rough estimates for the viscous and magnetic Reynolds numbers $\mathcal{O}(10^2)$–$\mathcal{O}(10^3)$. The latter depend on the model resolution and a posteriori estimates of the ratio of energy injection to dissipation length scales (Lesieur 1997).

All simulations begin from an unmagnetized ambient state in which small random velocity perturbation and seed magnetic field are introduced. A "spin-up" phase lasting up to 40 years is typically required to reach statistically stationary solutions.

2. RESULTS: MAGNETIC CYCLES

Figure 1 is a snapshot, in longitude–latitude Mollweide projection, of the radial component of the convective flow below the outer surface of the simulation domain. This flow exhibits the expected pattern of broad upflow cells delineated by a fragmented network of narrower downflow lanes, typical of thermal convection in a density-stratified environment (see Figure 5 in Miesch et al. 2000, and Figure 1 in Brun et al. 2004). Reynolds stresses associated with this stratified, rotating turbulent convection drive large-scale flows, including differential rotation and meridional circulation shown in Figure 2. The former is reasonably solar like, with equatorial acceleration and primarily latitudinal differential rotation at mid to high latitudes, vanishing rapidly within the stable layer underlying the SCZ. The latter evinces large flow cells in the equatorial regions, correlated with isocontours of angular velocity. From mid to high latitudes, the meridional flow is directed primarily poleward at the surface, and equatorward at the base of the convecting envelope, without significant penetration in the underlying stable layers. In the surface layers, the magnetic field is temporally and spatially intermittent, reaching locally values in excess of 0.1 T, but carries little net flux—the hallmark signature of turbulent small-scale dynamo action (Cattaneo 1999). However, below the base of the SCZ a strong and spatially well-organized large-scale component builds up, as shown in Figure 3. Significant turbulence persists at this depth, as a result of convective undershoot from above, so that the magnetic field still shows strong local fluctuations. Yet, a very well-defined large-scale component is clearly present, antisymmetric with respect to the equatorial plane, and reaching here strengths of ≃0.25 T. This compares well to the simulation results of Browning et al. (2006; Figure 2(B)) and

Q1

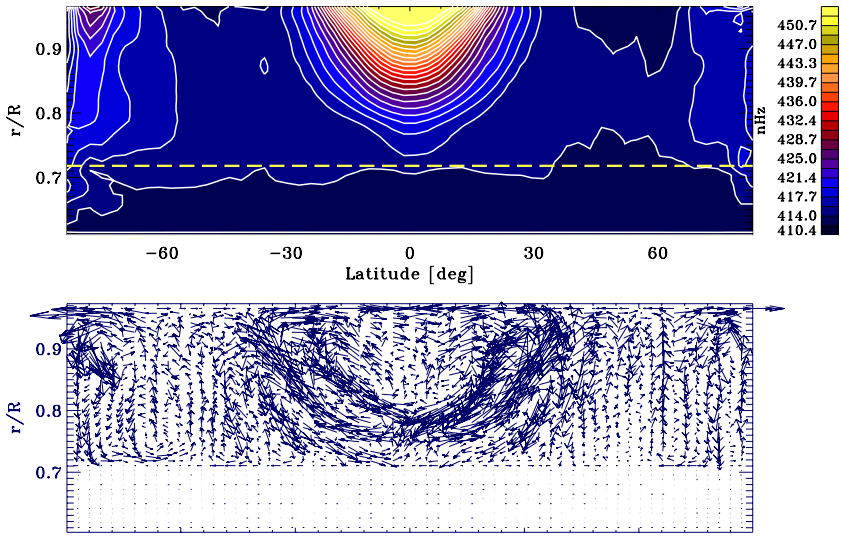

Figure 2. Large-scale flows building up in the simulation. Panel (A) shows a zonal and 1 year temporal average of angular velocity (top) plotted in the radius–latitude plane. Note the equatorial acceleration and rapid disappearance of differential rotation moving below the core–envelope interface (dashed line). Panel (B) shows the corresponding similarly averaged meridional flow. At mid to high latitudes, that flow is primarily poleward (∼2 m s^{-1}) at the surface and equatorward (∼0.5 m s^{-1}) at the core–envelope interface ($r/R = 0.718$).

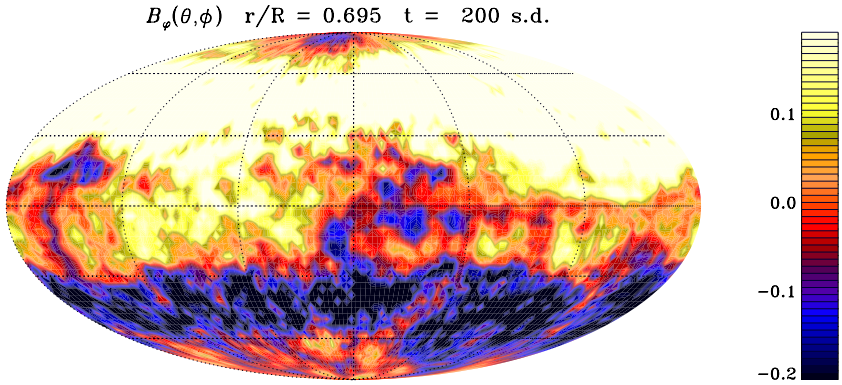

Figure 3. Toroidal component of the magnetic field, in the uppermost portion of the stable layer underlying the convective envelope ($r/R_\odot = 0.695$). A well-organized axisymmetric field component is evident, reaching 0.25 T in strength at mid-latitudes and showing antisymmetry about the equator. Although the snapshot is extracted in the nominally stable layer, convective undershoot from above induces strong fluctuations in the magnetic field.

supports their conclusion that a stably stratified tachocline-like layer is an essential component of a global solar-like large-scale dynamo (but see also Brown et al. 2010).

Our ILES simulations break into novel territory in that they exhibit regular polarity reversals on multi-decadal timescales, something that to the best of our knowledge had not yet been observed in global three-dimensional simulations of the SCZ operating in the turbulent regime. Figure 4 shows results of a low-resolution simulation ($128 \times 64 \times 47$) that was run for almost 255 years. Figure 4(A) shows a time–latitude diagram of the zonally averaged toroidal magnetic component extracted at the core–envelope interface in the simulation. Under the usual assumptions that sunspots do form following the buoyant rise and emergence of toroidal flux ropes formed and stored in the upper reaches of the tachocline, and that the number and the latitude of formation of these flux ropes are determined primarily by the strength of the large-scale toroidal magnetic field therein, this diagram is our simulation's analog to the well-known sunspot butterfly diagram. Several features are noteworthy. (1) The toroidal magnetic component undergoes fairly regular polarity reversals on a timescale of 30 years. This is three times the observed mean period of the solar cycle, but the fact that the simulation yields a cycle at all is already remarkable. (2) The large-scale magnetic component manages to retain a dipole-like polarity pattern throughout the whole simulation interval, again in agreement with inferences based on sunspot magnetic polarities. (3) The deep-seated toroidal magnetic field is concentrated at mid-latitudes, rather than the lower latitudes indicated by the sunspot butterfly diagram, but does show a hint of equatorward propagation in the course of each unfolding cycle. (4) Despite strong fluctuations in the amplitude and duration of individual cycles, the two solar hemispheres manage to retain a good level of long-term synchronicity in their spatiotemporal evolution. These characteristics are all solar-cycle-like.

Figure 4(B) shows time series of the zonally averaged toroidal magnetic flux density (B_T, solid lines) in each solar hemisphere, as color-coded, and of the polar cap radial magnetic flux density (B_P, dotted lines), again for each hemisphere. The former is calculated in a thin meridional slice straddling the core–envelope interface ($0.695 \leqslant r/R_\odot \leqslant 0.749$), and the latter at the top of the simulation domain over a cap extending 30° in latitude from the poles. These time series leave no doubt as to the global and cyclic nature of the large-scale dynamo mechanism. The apparent predominance of positive-signed toroidal flux densities, independently of hemisphere, can be traced to the

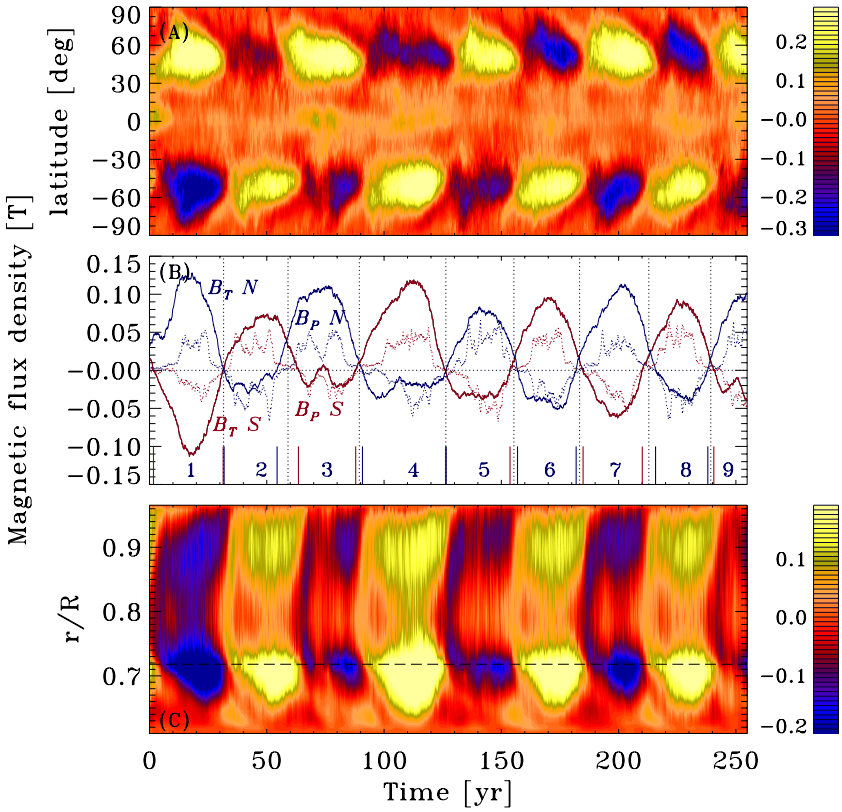

Figure 4. (A) Time–latitude "butterfly" diagram of the zonally averaged toroidal magnetic field component at $r/R_\odot = 0.718$. (B) Time series of the hemispheric tachocline toroidal flux densities (solid lines) and polar cap radial magnetic flux densities (dotted lines). The vertical line segments indicate the time of polarity reversals of the deep-seated toroidal component for each hemisphere, as color-coded. (C) Time–radius slice of the zonally-averaged toroidal magnetic field component extracted at mid-latitudes in the Southern hemisphere. The base of the nominally unstable layer is indicated by a horizontal dashed line. This statistically stationary solution underwent a prior "spin-up" phase lasting ∼40 years.

buildup of a persistent equatorially concentrated band of positive toroidal field, most prominent during simulated cycles 2 through 4 (see Figure 4(A)). The high degree of correlation between variations in the hemispheric polar cap fluxes indicates that the large-scale surface magnetic field is dominated by a dipole component approximately aligned with the rotation axis, and oscillating essentially in phase with the deep-seated toroidal component.

As can be seen in Figure 4(C), the cycle originates well within the SCZ, with the magnetic field undergoing further amplification once pumped down into the underlying stably stratified fluid layer, reaching there peak strengths in excess of 0.3 T for the stronger cycles. Field amplification also takes place in the upper half of the SCZ, but the toroidal field strength therein seldom exceeds 0.1 T. The signature of the magnetic cycle clearly pervades the whole SCZ, and also leaves its imprint on large-scale flows. Significant cycle-driven torsional oscillations are observed in the angular velocity. Counterrotating meridional flow cells also appear at very high latitudes in both hemispheres in the descending phase of most cycles. One such cell is just starting to appear in the Southern hemisphere in Figure 2(B), taken at a time corresponding to the peak of the first cycle in Figure 4.

3. THE PHYSICAL NATURE OF THE LARGE-SCALE DYNAMO PROCESS

The simultaneous presence of a well-defined dipole moment and of a Reynolds-stress-driven axisymmetric mean differential rotation sustained throughout the simulation suggests that the simulation may be operating as what is known in mean field theory as an $\alpha\Omega$ dynamo, with the regeneration of the poloidal magnetic component taking place through the agency of the so-called α-effect, more precisely, the $\alpha_{\phi\phi}$ component of the alpha tensor. Calculation of the zonal component of the mean electromotive force (EMF), with the fluctuating components of the flow and field computed by subtracting the zonal averages, does yield a well-defined hemispheric pattern of like-signed EMF in both hemispheres, reversing in step with the axisymmetric dipole moment, consistent with a positive α-effect in the bulk of the SCZ, producing a positive dipole moment from a toroidal component positive in the Northern hemisphere, as shown in Figure 4(B). A similar qualitative correspondence with the behavior predicted by mean field theory was also noted by Käpylä et al. (2010) in their spherical wedge convective dynamo simulations.

It remains to be understood why our simulations manage to produce regular polarity reversals, while those of Browning et al. (2006) by all appearances do not. Both simulations are very similar in design and reach comparable turbulent and magnetic intensities, at least judging from the convective flow speeds, strengths of mean magnetic field in stable layer, surface field strengths, ratio of total magnetic to kinetic energies, etc. However, our ILES approach allows us to reach a turbulent state at relatively low spatial resolution, which in turn permits longer temporal integrations in reasonable wallclock time. It is certainly possible that the lack of polarity reversals in the Browning et al. (2006) simulations is a simple consequence of their relatively short integration time.

One notable modeling difference is a weak thermodynamic forcing used in our experiments, with entropy perturbations merely redistributed and weakly damped while maintaining the ambient state. Another is our use of a boundary condition on the magnetic field that allows magnetic helicity to exit the domain, which is believed to be more conducive to large-scale dynamo action (see, Käpylä et al. 2008; Brandenburg 2009 and references therein). At a more fundamental level, it is also quite possible that the behavior of the simulation at small spatial scales plays a key role in governing large-scale dynamo action. The latter can be viewed as a combination of forward and inverse cascades, of both magnetic energy and helicity, operating from the energy injection (intermediate) scale to both the (small) dissipative scales and the (large) dynamo scales. Varying treatment of the manner small scales are treated can affect the inverse cascades, especially if an insufficient separation of scales is realized in the simulation between the dissipative and energy injection scales. The numerical experiments of Elliott & Smolarkiewicz (2002) on purely hydrodynamical solar convection offer empirical support to this conjecture.

This Letter has focused on the general characteristics of the solar-like cycles of the large-scale magnetic component building up in MHD ILES of the SCZ. There are of course many additional simulation features that are of interest and need to be explored in detail. In particular, our preliminary analyses reveal a weak but clear signature of the magnetic cycle in the heat transport throughout the convective envelope. This has direct relevance to the ongoing debate regarding the ultimate origin of the observed decadal variations of the total solar irradiance during the magnetic activity cycle.

The numerical simulations reported in this Letter were carried out primarily on the computing facilities of the Réseau Québécois de Calcul de Haute Performance. This work is supported by Canada's Natural Sciences and Engineering Research Council, Research Chair Program, and Foundation for Innovation (P.C.). The National Center for Atmospheric Research is supported by the National Science Foundation (P.K.S.).

REFERENCES

Brandenburg, A. 2009, Space Sci. Rev., 144, 87
Brown, B. P., Browning, M. K., Brun, A. S., Miesch, M. S., & Toomre, J. 2010, ApJ, 711, 424
Browning, M. K., Miesch, M. S., Brun, A. S., & Toomre, J. 2006, ApJ, 648, L157
Brun, A. S., Miesch, M. S., & Toomre, J. 2004, ApJ, 614, 1073
Cattaneo, F. 1999, ApJ, 515, L39
Domaradzki, A., Xiao, Z., & Smolarkiewicz, P. K. 2003, Phys. Fluids, 15, 3890
Elliott, J. R., & Smolarkiewicz, P. K. 2002, Int. J. Numer. Methods Fluids, 39, 855
Glatzmaier, G. A. 1984, J. Comput. Phys., 55, 461
Käpylä, P. J., Korpi, M. J., & Brandenburg, A. 2008, A&A, 491, 353
Käpylä, P. J., Korpi, M. J., Brandenburg, A., Mitra, D., & Tavakol, R. 2010, Astron. Nachr., 331, 73
Lesieur, M. 1997, Turbulence in Fluids (Dordrecht: Kluwer), 515
Miesch, M. S., & Toomre, J. 2009, Annu. Rev. Fluid Mech., 41, 317
Piotrowski, Z. P., Smolarkiewicz, P. K., Malinowski, S. P., & Wyszogrodzki, A. A. 2009, J. Comput. Phys., 228, 6268
Prusa, J. M., & Smolarkiewicz, P. K. 2003, J. Comput. Phys., 190, 601
Prusa, J. M., Smolarkiewicz, P. K., & Wyszogrodzki, A. A. 2008, Comput. Fluids, 37, 1193
Smolarkiewicz, P. K., Grubišić, V., & Margolin, L. G. 1997, Mon. Weather Rev., 125, 647
Smolarkiewicz, P. K., & Szmelter, J. 2009, J. Comput. Phys., 228, 33
Smolarkiewicz, P. K., Temperton, C., Thomas, S. J., & Wyszogrodzki, A. A. 2004, Proc. ECMWF Seminar Series, Reading, 203
Waite, M. L., & Smolarkiewicz, P. K. 2008, J. Fluid Mech., 606, 239

Queries

Page 2

Q1

Author: Please include reference "Miesch et al. (2000)" in the reference list or else delete it from the text.

Page 5

Q2

Author: Please check the sense of the sentence "Varying treatment of the manner small scales are treated can . . ." since it seems to be unclear.

Q3

Author: Please check the details for any journal references that do not have a pale purple link (CrossRef doi) or a blue link (NASA ADS or arXiv e-print). A journal reference with no links may contain some incorrect information.

Q4

Author: Please check whether the publisher location in reference "Lesieur (1997)" is correct as included.

Q5

Author: Please provide publisher's details in reference "Smolarkiewicz et al. (2004)."

Online-only colour figures

This proof PDF is identical in specification to the PDF file that will be published in the online journal. To view any online-only color figures as they will appear in the printed journal, we recommend that this color PDF file be printed on a black & white printer.